Supporting Information

Malito et al. 10.1073/pnas.1419686111

SI Materials and Methods.

Cloning, Expression, and Purification. PCR products encoding NadA proteins with a 6His tag at the C terminus were cloned using the polymerase incomplete primer extension cloning method (1) in the pET21b$^+$ expression vector (Novagen). After sequencing, each plasmid was transformed into *E. coli* BL21 (DE3) cells (Novagen) for protein production. Expression of NadA constructs was performed either in rich medium (LB) at 30 °C or in high-throughput complex medium 3 [30 g/L yeast extract, 15 g/L glycerol, 20 g/L K_2HPO_4, 5 g/L KH_2PO_4, 0.5 g/L $MgSO_4$ (pH 7.2)] at 27 °C for 30 h. Purifications were performed by nickel affinity using HisTrap, Q HP anion exchange, and preparative size-exclusion chromatography [Superdex 75 (16/60)] columns (GE Healthcare) in final buffer containing 20 mM Tris·HCl, 150 mM NaCl (pH 8.0). Sample purity was assessed by reverse-phase HPLC, and integrity was determined on an analytical size-exclusion HPLC TSG G3000SWxl column (Tosoh Bioscience).

Crystallization, Data Collection, and Structure Determination. Crystallization experiments were performed by the sitting-drop method, using 96-well low-profile crystallization plates, mixing equal volumes (0.2 μL) of proteins at ∼20 mg/mL and reservoir solutions from six different commercial screens. Initial crystal hits appeared after 4 wk for construct NadA4$_{D24–R219}$, from condition E10 of the Hampton Research PEG/ION screen containing 8% Tacsimate (pH 4.0) and 20% PEG3350. These crystals dissolved in their original drop at 20 °C over 30 d of incubation. Optimization using pH gradients of Tacsimate, concentration gradients for both Tacsimate and PEG3350 and protein concentration led to reproducible crystals using 10% Tacsimate (pH 4.0), 20% PEG3350. Further crystallization screens were performed using the additive screen from Hampton Research. Before data collection, several crystals were soaked in different cryoprotectant solutions and were cooled to 100 K in liquid nitrogen; the best results were obtained using 10–20% ethylene glycol. Diffraction screenings of more than 100 crystals of NadA4$_{D24–R219}$ resulted in one native dataset collected at ∼4 Å resolution. The overall quality of this dataset was very low, because it was affected by disorder and severe anisotropy and with space group *P*1. Because of the weak sequence similarity with available TAA structures found in the PDB, we were not able to solve the structure of NadA4$_{D24–R219}$ using this initial native dataset by molecular replacement. Also, because of the absence of any Met or Cys residues in the sequence of NadA, we attempted soaks of heavy atoms and halides. However, the low-resolution diffraction, intrinsic disorder, and anisotropy of these crystals did not allow us to measure significant anomalous signals.

Although the overall quality of these initial crystals of NadA4$_{D24–R219}$ could not be improved notably by further optimization steps, the use of construct NadA5$_{D24–R220}$ under the same conditions with 10% Tacsimate (pH 4.0) and 20% PEG3350 immediately yielded improved crystals, as judged by inspection under the microscope. Furthermore, the use of additive screens allowed us to obtain numerous crystals of NadA5$_{D24–R220}$ that were shaped as elongated plates with the approximate dimensions 800 × 140 × 50 μm. An initial native dataset at 2.0-Å resolution was collected on a crystal of the NadA5$_{D24–R220}$ construct with excellent overall quality and space group *R* 3 2 (H). In this case, also, we were not able to solve the structure of NadA5$_{D24–R220}$ by molecular replacement, prompting us to use heavy atoms and halide soaking for experimental de novo phasing by SAD or MAD. Soaking experiments were performed using solutions containing a slightly more concentrated crystallization mother liquor, made of 12% Tacsimate (pH 4.0) and 22% PEG 3350, supplemented with variable concentrations of derivatives from the lanthanide phasing kit from NatX-ray, the Magic Triangle phasing kit from Jena Bioscience, or manually made stock solutions of NaI, NaBr, KI, and KBr. Incubation times varied from a few seconds up to 5 min, and concentrations of soaked derivatives varied from 100 mM to 1 M. All crystals used for soaking experiments then were back-washed in mother liquor and cryoprotectant (10–20% ethylene glycol) before freezing in liquid nitrogen to ensure that no unspecific, unbound, heavy atoms or halides were present that could interfere with the measurement of anomalous signal. Although fluorescence scans on bromine- and lanthanide-soaked crystals confirmed the incorporation of derivatives in several crystals, derivative datasets from these crystals collected at their respective edges did not allow structure determination. However, data collections of crystals soaked in 1 M sodium iodide performed at a wavelength of 1.54 Å to maximize the anomalous signal while reducing radiation damage resulted in one derivative dataset at 2.05-Å resolution. These data were processed with XDS (2), resulting in an overall R_{sym} of 6.2% (last shell 82.6%) and overall anomalous correlation of 54% extending well up to 2.6 Å (correlation of 26%).

The structure of NadA5 was solved by the SAD method. Substructure solution, phasing, density modification, and initial model building were performed in autosol, phaser, and autobuild of the Phenix suite (3). Subsequent rebuilding and refinement were performed with Coot (4) and phenix.refine; all other crystallographic manipulations were carried out in CCP4 (5). All crystallographic software was compiled, installed, and maintained by SBGrid (6). The calculated Matthews coefficient of the crystals of NadA5$_{D24–R220}$ was 3.12 Å^3/Da, which corresponds to a solvent content of 60% with one molecule of NadA5$_{D24–R220}$ occupying the asymmetric unit. Each single chain of NadA5$_{D24–R220}$ sits on a threefold crystallographic axis, so that two additional symmetry-related molecules are positioned to complete the biological homotrimer. The final refined model of NadA5$_{D24–R220}$ has R_{work}/R_{free} of 18.2/20.7, excellent geometry, a low clash score, and all residues within the Ramachandran favored region. All data collection and refinement statistics are reported in Table S1. Atomic coordinates have been deposited in the PDB with ID code 4CJD.

Negative Stain TEM. A 5-μL aliquot of the native, tagless NadA3$_{Δ351–405}$ diluted to 0.02 mg/mL was used, loaded onto a glow-discharged 200-square mesh copper/nickel grid coated with a thin carbon film, and allowed to stand for 2 min. Excess solution was blotted off with Whatman filter paper no. 1 (Whatman International Ltd.). The grids first were washed by streaming several drops of ddH_2O over the grids and then were negatively stained with a solution of 1% buffered uranyl acetate (pH 4.5) for 50 s. The excess liquid was soaked off by Whatman filter paper no. 1, and the grid was left to air dry. The grids were observed using a TEM Tecnai G2 spirit transmission electron microscope (FEI) operating at 80 kV set in low-dose conditions and a magnification of 220,000×. Images were collected with an Olympus SIS Morad 2K*4K CCD camera. Images taken at 220,000× magnification first were analyzed for defocus (1.1–3.2 μm) and contrast transfer function (CTF) using the Medical Research Council program CTFFIND3 (7). Single NadA3 particles were picked semiautomatically from digitized images using the Boxer tool from the EMAN software package (8). Direct measurement of NadA3 homotrimers using command-measure from the EMAN software (9, 10) clearly showed that the homotrimeric

structure displayed size homogeneity. Image phases were corrected for the effect of the CTF in IMAGIC 5 (11) at a box of 100 × 100 pixels (corresponding to a box of 146 × 146 Å and a step size of 1.46 Å per pixel in IMAGIC5).

***In Silico* Molecular Modeling of Full-Length NadA3 and NadA5.** Once the translocation domains of NadA3 and NadA5 were threaded onto the coordinates of Hia (PDB code 3EMO) (12), the NadA5 stalk was extended to include residues 138–220 that were not observed in the crystal structure by using the coordinates of its N-terminal coiled-coil (residues 27–137) as a template. The coiled-coil heptad *a–g* periodicity observed in the structure was used as a reference to align the NadA sequence to be modeled in frame with the sequence of the template. The final model of NadA5 includes residues 27–137, corresponding to those observed in the crystal structure, 147–161, and 186–324, with gaps of fragments 136–156 and 162–185 that correspond to regions of low probability or unclear coiled-coil periodicity. The experimental crystallographic structure of NadA5 then was used as a template to model fragment 27–170 of NadA3, which from sequence alignment corresponds to the visible coiled-coil (27–137) of NadA5 with the addition of one long insertion (residues 106–137, NadA3 numbering) starting at residue 104 (NadA5 numbering). The stalk region of NadA3 then was extended to residue 330 following the procedure described for NadA5. However, as for NadA3, regions where the coiled-coil probability was low (namely, residues 105–107, 151–160, 218–223, and 267–287) were omitted. Both full-length models were subjected to manual refinement to eliminate major steric clashes on side chains and then to energy minimization with the Gromos 43B1 force field (13).

Antibody Generation and Fab Purification. Purified recombinant NadA protein from serogroup B *N. meningitidis* strain MC58 was used to immunize 4- to 6-wk-old female CD1 mice. The first dose was a 50-μg injection with Freund's complete adjuvant; the second, third, and fourth doses, at days 14, 21, and 33, were 25 μg each administered with Freund's incomplete adjuvant. After 1 wk (on day 39), anti-NadA titers were measured in mice sera using ELISA plates coated with the purified recombinant protein and anti-IgG, anti-IgG2a, or anti-IgG2b as the secondary antibodies. A fifth dose was administered without adjuvant, and the mice were killed 5 d later. Their spleen cells were fused with myeloma cells (NS0). After a 2 wk incubation in hypoxanthine-aminopterin-thymidine selective medium, the hybridoma supernatants were screened for antibody-binding activity by ELISA. Hybridomas secreting anti-NadA antibodies selected on the basis of the results obtained by SBA and FACS analysis in Novartis were cloned by limiting dilution and then were expanded and frozen for subsequent purification of mAbs. The supernatants of the subclones were sent to Novartis for a second screening by SBA and FACS analysis of the hybridomas to be expanded for the purification of mAb. mAb 33E8 was purified from culture supernatant by Protein G affinity columns (GE Healthcare), and after exhaustive dialysis in PBS buffer the concentration was determined by spectrophotometric reading at 280 nm. The mAb subclass was determined using a mouse mAb isotyping kit (Roche).

SPR. For the single-cycle kinetics (SCK) experiments, which are well suited for the measurement of high-affinity binding events (14), a commercially available Mouse Antibody Capture Kit (GE Healthcare) was used to immobilize rabbit anti-mouse antibodies by amine coupling on a carboxymethylated dextran sensor chip (CM-5; GE Healthcare). An IgG density level yielding ∼10,000 response units (RUs) was prepared. The rabbit anti-mouse IgG was used to capture ∼600 RU mAb 33E8 (molecular mass ∼150 kDa); the mAb capture was highly stable, resulting in a dissociation drift of <2 RU/h. Experimental running buffer contained 10 mM potassium phosphate, 150 mM NaCl, and 0.05% (vol/vol) P20 surfactant (pH 7.4). To determine the equilibrium K_d and kinetic parameters, a titration series of five consecutive injections of increasing analyte concentration (maximum concentration of 10, 50, and 5,000 nM for the clones 24-342, 24-170, and 24-89, respectively; flow rate of 30 μL/min) followed by a single final surface-regeneration step with buffer containing 10 mM glycine (pH 1.7) (flow rate of 10 μL/min) was performed using the standard SCK method (14) implemented by Biacore T200 Control Software (GE Healthcare). For initial comparisons of NadA constructs and variants binding to captured mAb 33E8, single equimolar injections of NadA proteins at a concentration of 100 nM were performed with a flow rate of 30 μL/min. An anti-mouse antibody–coated surface without captured mAb 33E8 was used as the reference channel. A blank injection of buffer only was subtracted from each curve, and reference sensorgrams were subtracted from experimental sensorgrams to yield curves representing specific binding. The data shown are representative of at least two independent experiments. SPR data were analyzed using the Biacore T200 Evaluation software (GE Healthcare). SCK experiments were performed in duplicate, and each sensorgram was fitted with the 1:1 Langmuir binding model, including a term to account for potential mass transfer, to obtain the individual k_{on} and k_{off} kinetic constants; the individual values then were combined to derive the single averaged K_d values reported. Additional details of SPR data analysis have been reported previously (15).

Complement-Mediated Bactericidal Activity. *N. meningitidis* strains were grown overnight on chocolate agar plates (Biomerieux) at 37 °C, 5% CO_2, and then were used to inoculate 7 mL of Muller–Hinton broth medium supplemented with 0.25% glucose to reach the OD_{600} of ∼0.05. Cultures were incubated for ∼2 h at 37 °C with shaking until early log phase (OD_{600} of ∼0.25). The bactericidal activity of mAbs was evaluated against strains DE11445, 5/99, and NMB, which express NadA variants 1, 2, and 3, respectively. Early log-phase cultures of bacteria were diluted in Dulbecco's PBS (Sigma) containing 1% BSA and 0.1% glucose (assay buffer) at a working dilution of 10^4–10^5 cfu/mL. Bacteria were incubated with serial twofold dilutions of test mAb (0.25–0.0005 μg/mL) and 25% baby rabbit complement (Cederlane).

Flow Cytometry-FACS. *N. meningitidis* strains DE11445, 5/99, NMB, and IB4846, carrying NadA variants 1, 2, 3, and 5, respectively, were grown overnight on chocolate agar plates (Biomerieux) at 37 °C, 5% CO_2. Colonies were picked from the overnight plate and suspended in Muller–Hinton broth until the OD_{600} reached ∼0.5. Then 1 mL of suspension was centrifuged, and the bacterial pellet was suspended in PBS plus 1% BSA. Fifty microliters of suspended bacteria were incubated for 1 h with 10 μg/mL mAb in a reaction volume of 100 μL. The binding of mAb 33E8 was detected using an anti-mouse (whole-molecule) FITC-conjugated antibody (Sigma) at a 1:100 dilution. All incubations were performed at room temperature. Before flow cytometry analysis, bacteria were fixed with 0.5% formaldehyde in PBS buffer for 1 h. A polyclonal serum from mice immunized with NadA variant 3 was used as positive control at a dilution of 1:100, and bacteria incubated with PBS plus 1% BSA were used as negative control.

Nondenaturing Nanoelectrospray MS. NadA samples were buffer exchanged against 250 mM ammonium acetate (pH 8.0) using Zeba spin desalting columns with a 7-kDa molecular mass cutoff (Thermo Scientific). A SynaptG2 HDMS mass spectrometer (Waters) equipped with a nano-ESI source was used, and the instrument was calibrated in resolution mode (m/z 500−9,000) using a 100 mg/mL cesium iodide solution. Spectra were acquired in positive mode for 5–30 min to obtain a good signal-to-noise

ratio and were processed with MassLynx 4.1 software with minimal smoothing.

Epitope Mapping by Synthetic Peptide Scanning. One hundred twenty distinct peptides, each of 13 residues, with a neighbor overlap of 10 residues, and representing the entire mature NadA3 ectodomain protein were synthesized and spotted onto nitrocellulose membranes, and mAb 33E8 was coincubated with the library. An alkaline phosphatase-conjugated goat anti-mouse antibody was used for detection of binding.

Epitope Mapping by HDX-MS. Deuterium oxide (99.9 atom % D), sodium deuteroxide, deuterium chloride, acetonitrile, and Glu-fibrinogen peptide were all purchased from Sigma Aldrich and used without further purification.

Sample preparation for HDX-MS analysis. The antigen/Fab complex was formed by adding 200 pmol of NadA to the Fab, using a molar ratio of 1:1, first incubated for 30 min at room temperature and then for 10 min on ice before the deuteration was performed on ice. The labeling reactions were performed on ice by adding the proper deuterated buffer (PBS with a pD of 7.4), reaching a deuterium excess of 82.6%. Over the time course of the experiment (ranging from 30 s to 30 min), 30 μL of the sample were removed and quenched with the same volume of an ice-cold 200 mM sodium phosphate buffer (added with 4 M guanidinium chloride) to dissociate the antigen/Fab complex and to lower the pH to 2.4. The quenched aliquots were frozen immediately in liquid nitrogen and stored at −80 °C for less than 24 h. A control experiment without Fab was prepared using the conditions previously described (PBS was used instead of the antibody preparation).

Local HDX-MS analysis. Labeled samples were thawed rapidly to 0 °C and injected into a Waters nanoACQUITY ultra-performance liquid chromatographic (UPLC) system with HDX technology. The injector, switching valve, columns, solvents, and all associated tubing were at 0 °C to limit back-exchange. For local HDX-MS, protein samples were digested online for 2.5 min at 20 °C with a flow rate of 200 μL/min using a Poroszyme Immobilized Pepsin Cartridge (2.1 × 20 mm; Applied Biosystems) equilibrated with 100% buffer A (0.1% formic acid in water). The generated peptides were trapped immediately, concentrated, and desalted using a VanGuard BEH Precolumn (1.7 μm, 2.1 × 5 mm; Waters). Peptides then were separated on an ACQUITY UPLC BEH C18 reverse-phase column (1.7 μm, 1.0 × 100 mm; Waters) with a linear gradient from 15–45% solvent B [acetonitrile/water (9:1), 0.1% formic acid] over 6.8 min at 40 μL/min.

Mass spectra acquisition and interpretation. Mass spectra were acquired in resolution mode (m/z 100–2,000) on a Waters SynaptG2 mass spectrometer equipped with a standard ESI source. Mass accuracy was ensured by continuously infusing a Glu-Fib solution (600 fmol/μL in 50% acetonitrile, 0.1% formic acid) through the reference probe of the ESI source. The identity of each peptide was confirmed by mass spectrometry elevated energy (MS^E) analyses. MS^E was performed directly by a succession of low-collision (6-V) and high-collision (25-V) energies in the transfer region of the mass spectrometer. All fragmentations were performed using argon as the collision gas. Data were processed using Protein Lynx Global Server 2.5 (Waters), and each fragmentation spectrum was inspected manually to confirm the assignment. The DynamX software (Waters) was used to select the peptides considered for the analysis and to extract the centroid mass of each of them and for each charge state as a function of the labeling time. Only the peptic peptides present in at least three repeated digestions of the unlabeled proteins were considered for the analysis.

1. Klock HE, Koesema EJ, Knuth MW, Lesley SA (2008) Combining the polymerase incomplete primer extension method for cloning and mutagenesis with microscreening to accelerate structural genomics efforts. *Proteins* 71(2):982–994.
2. Kabsch W (2010) Xds. *Acta Crystallogr D Biol Crystallogr* 66(Pt 2):125–132.
3. Adams PD, et al. (2010) PHENIX: A comprehensive Python-based system for macromolecular structure solution. *Acta Crystallogr D Biol Crystallogr* 66(Pt 2):213–221.
4. Emsley P, Cowtan K (2004) Coot: Model-building tools for molecular graphics. *Acta Crystallogr D Biol Crystallogr* 60(Pt 12 Pt 1):2126–2132.
5. Collaborative Computational Project, Number 4 (1994) The CCP4 suite: Programs for protein crystallography. *Acta Crystallogr D Biol Crystallogr* 50(Pt 5):760–763.
6. Morin A, et al. (2013) Collaboration gets the most out of software. *eLife* 2:e01456.
7. Mindell JA, Grigorieff N (2003) Accurate determination of local defocus and specimen tilt in electron microscopy. *J Struct Biol* 142(3):334–347.
8. Ludtke SJ, Baldwin PR, Chiu W (1999) EMAN: Semiautomated software for high-resolution single-particle reconstructions. *J Struct Biol* 128(1):82–97.
9. Ludtke SJ (2010) 3-D structures of macromolecules using single-particle analysis in EMAN. *Methods Mol Biol* 673:157–173.
10. Tang G, et al. (2007) EMAN2: An extensible image processing suite for electron microscopy. *J Struct Biol* 157(1):38–46.
11. van Heel M, Harauz G, Orlova EV, Schmidt R, Schatz M (1996) A new generation of the IMAGIC image processing system. *J Struct Biol* 116(1):17–24.
12. Meng G, St Geme JW III, Waksman G (2008) Repetitive architecture of the Haemophilus influenzae Hia trimeric autotransporter. *J Mol Biol* 384(4):824–836.
13. Scott WR, et al. (1999) The GROMOS biomolecular simulation program package. *J Phys Chem A* 103(19):3596–3607.
14. Karlsson R, Katsamba PS, Nordin H, Pol E, Myszka DG (2006) Analyzing a kinetic titration series using affinity biosensors. *Anal Biochem* 349(1):136–147.
15. Karlsson R (1999) Affinity analysis of non-steady-state data obtained under mass transport limited conditions using BIAcore technology. *J Mol Recognit* 12(5):285–292.
16. Strelkov SV, Burkhard P (2002) Analysis of alpha-helical coiled coils with the program TWISTER reveals a structural mechanism for stutter compensation. *J Struct Biol* 137(1-2):54–64.

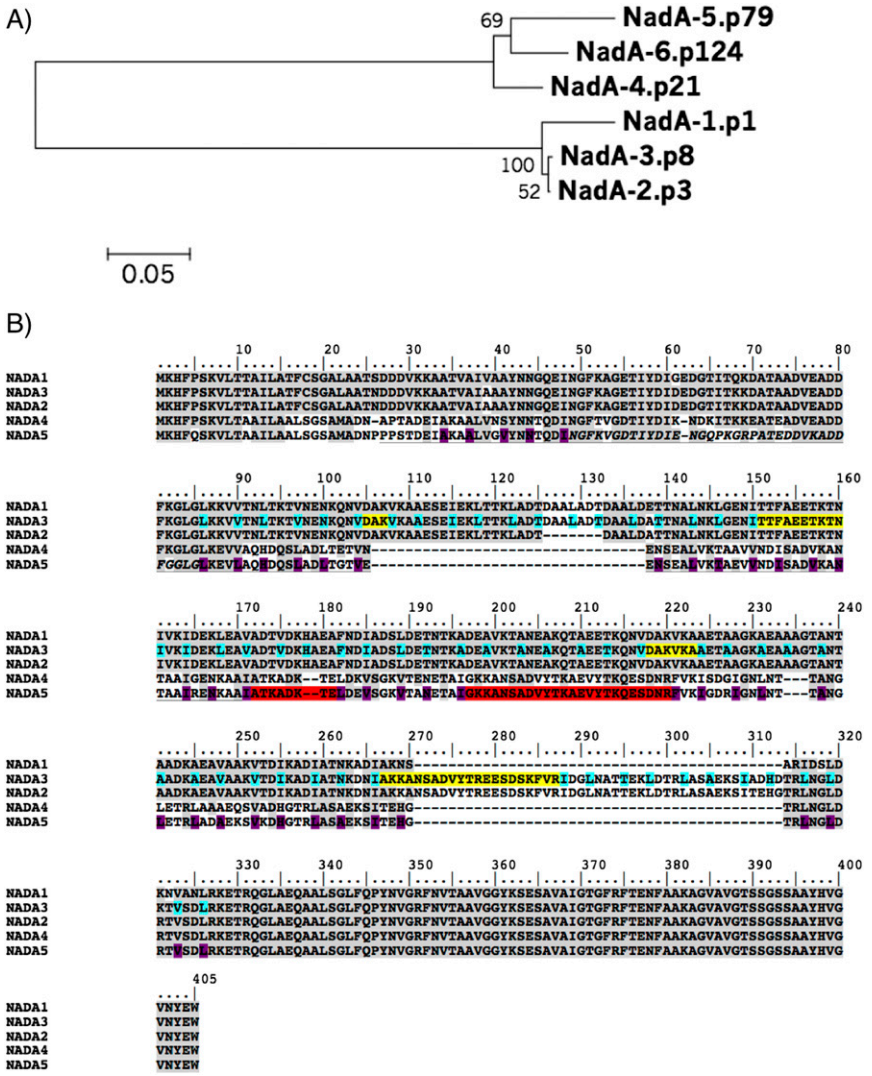

Fig. S1. NadA sequence variants and alignment. (*A*) The neighbor-joining tree reconstructed using the bootstrap test of phylogeny of six different amino acid sequences shows the subdivision of NadA protein variants in two groups, with NadA1, 2, and 3 in one group and NadA4, 5 and 6 in the other group. (*B*) Sequence identities between NadA variants are shown in gray shades. The regions of NadA5 observed in the crystal structure of fragment A24–R220 are underlined, and the insertion forming the wing-like structures is underlined and in italic font. The observed (between residues A34 and A137) and predicted (between residues 138 and 245) coiled-coil periodicity of NadA5 is shown by dark purple shading for residues in *a* and *d*, and predicted coiled-coil periodicity of NadA3 is shown with cyan shading. Yellow and red shading indicates segments of the coiled-coil regions of NadA3 and NadA5, respectively, where sequences with coiled-coil periodicity are lacking.

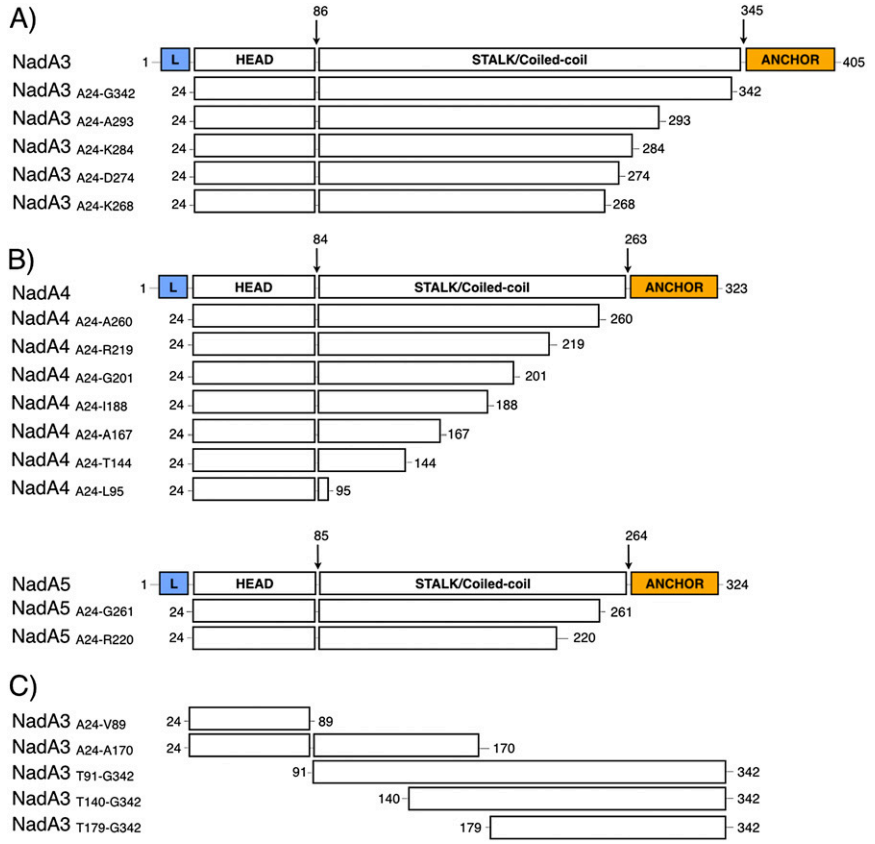

Fig. S2. Domain organization and constructs of NadA. All constructs of NadA3, 4, and 5 used for thermostability and structural studies are shown in *A* and *B*. Constructs of NadA3 used for epitope mapping are shown in *C*. Each expression construct had a C-terminal 6His tag to enable affinity purification. The predicted domain organization and domain boundaries as detected by sequence analyses and sequence similarities with other TAAs are shown schematically.

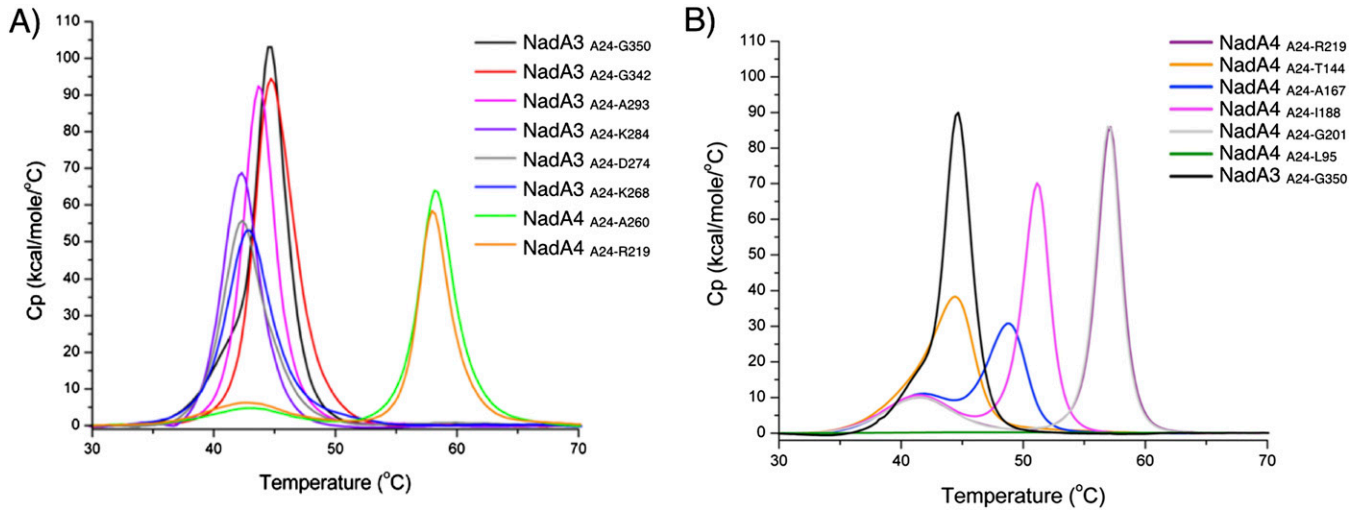

Fig. S3. Thermostability of NadA variants with variable coiled-coil length. (*A*) DSC profiles of initial NadA3 and NadA4 constructs. (*B*) Thermostability of NadA4 constructs with a progressively reduced C-terminal coiled-coil and of an NadA "head-only" construct.

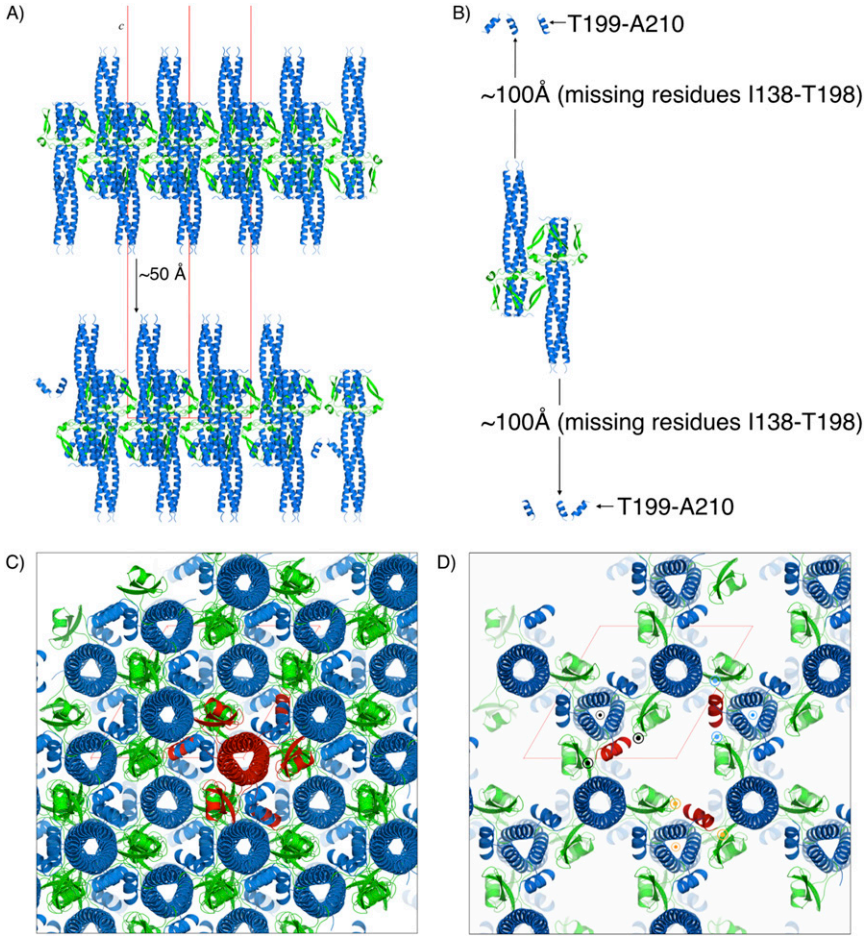

Fig. S4. Crystal packing of NadA5. (*A*) NadA5 trimers are arranged in antiparallel columns along the *c* axis of the crystal. Shown here is a section of the content of the unit cell of crystals of NadA5 (*bc* face). NadA is depicted as a cartoon in which the coiled-coil/stalk region is colored blue and the wing-like structures of the head domain are colored green. The stalks of symmetry-related trimers run in opposite directions toward a region of very few crystal contacts corresponding to the gap of unobserved or disordered residues (I138–T198) and resulting in an unusual discontinuity of crystal packing covering a distance of ~50 Å. The section of the coiled-coil (residues I138–T198) that could not be adequately fitted because of low-σ electron density clearly bridges this gap in the crystal packing. (*B*) Two symmetry-related antiparallel trimers of NadA5 are shown to highlight the arrangement and contacts mediated by the head-like domain. The uncoiled C-terminal short fragments are also shown. (*C*) View from top (*ab* face) of the crystal packing of NadA5 showing one trimer as a red cartoon and all other trimers colored as in *A* and *B*. (*D*) Slab view of *C* to highlight the position of the wing-like structures (green) of three parallel NadA trimers that sandwich each of the three unwound short helices (red) made of residues T199–A210. Three trimers of NadA5 oriented from N→C toward the viewer and their wing-like structures of the head that sandwich the short C-terminal fragments of a successive symmetry-related trimer are marked with circled dots colored black, blue, and orange. Faint red lines in *A*, *C*, and *D* show the unit cell. All structure figures were generated using PyMOL (www.pymol.org).

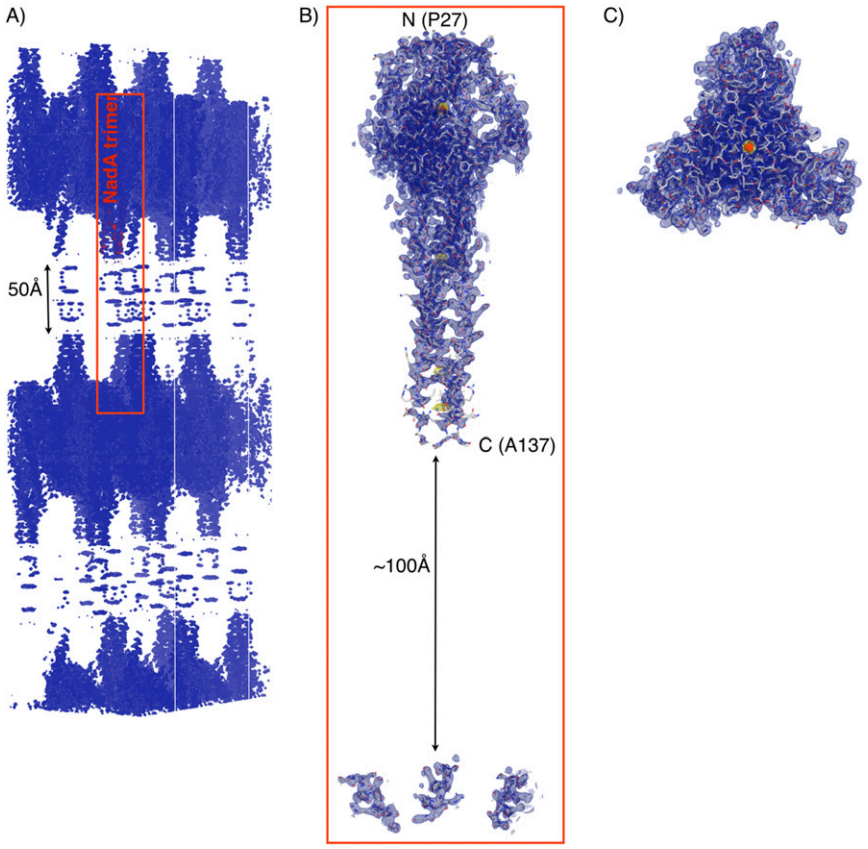

Fig. S5. Electron densities of NadA5. (*A*) Initial 2*Fo-Fc* electron density maps after phasing and density modifications contoured at 0.8σ are shown for a portion of the unit cell as blue mesh. The region within the red box is occupied by a trimer of NadA (labeled). (*B* and *C*) Zoomed-in views of the region occupied by a trimer of NadA showing 2*Fo-Fc* electron density maps after full refinement of the structure contoured at 1σ from a lateral (*B*) and top (*C*) view. In both *B* and *C*, anomalous difference maps contoured at 5σ are shown as yellow mesh around red spheres that depict iodides.

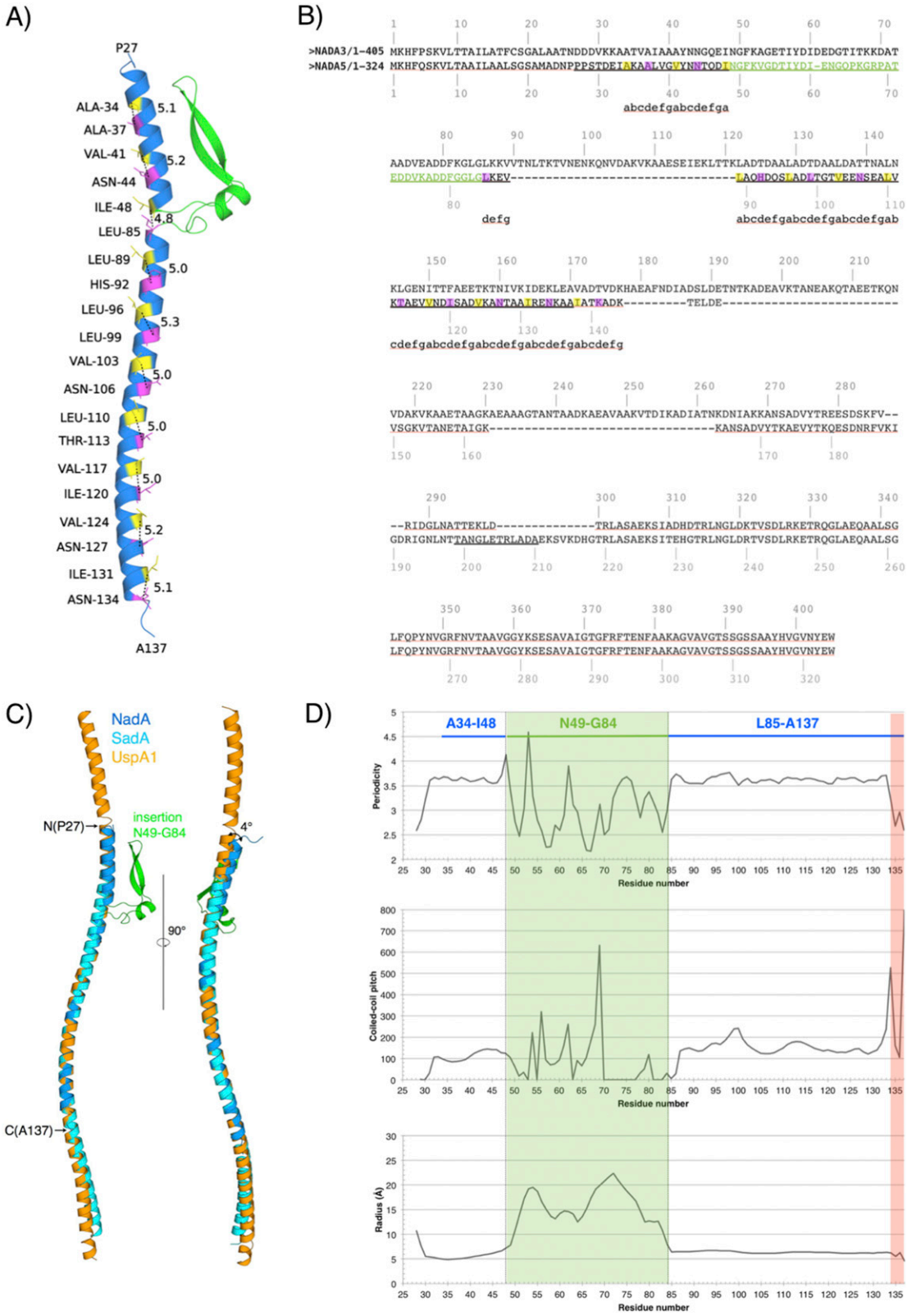

Fig. S6. The coiled-coil of NadA5. (*A*) Details of monomeric NadA5, with side chains occupying positions *a* and *d* of the canonical heptad repeat depicted as yellow and magenta sticks, respectively. Cα–Cα distances between residues *a* and *d* are shown by black dashes, and distances (in angstroms) are labeled. (*B*) Sequence alignment between NadA3 and NadA5, with the location of the heptad repeats of the coiled-coil observed in the crystal structure of NadA5 marked below the sequence with the motifs *abcdefg*, and with *a* and *d* in yellow and magenta boxes, respectively. Residues belonging to the insertion between residues 49 and 84, which make the wings of the head, are shown with green fonts. (*C*) Structural comparison between NadA5 (blue and green cartoon), SadA (PDB 2WPQ) (cyan), and UspA1 (PDB 2QIH) (orange). Optimal superpositions were obtained when matching Cα atoms of residues N106–A137 of NadA5 onto

Legend continued on following page

N488–S519 of SadA, and N601–D632 of UspA1, which align coiled-coil heptad repeats by keeping fixed an Asn of N@*d* layers found in all three structures. These superpositions result in rmsd values of 0.54 Å and 0.57 Å for SadA and UspA1, respectively, and in a deviation of ∼4° in the helical angle of the superposed helices. (*D*) Plots of the coiled-coil periodicity (*Top*), pitch (*Middle*), and radius (*Bottom*) of the observed fragment P27–A137 of NadA5, calculated with the program TWISTER (16) and shown as a function of residue number. The green-shaded region corresponds to the insertion of residues N49–G84, and the region shaded in red shows deviations of the geometry of the coiled-coil nearby residues N134 and K135; these deviations likely are induced by the lack of coiled-coil periodicity immediately toward the C terminus.

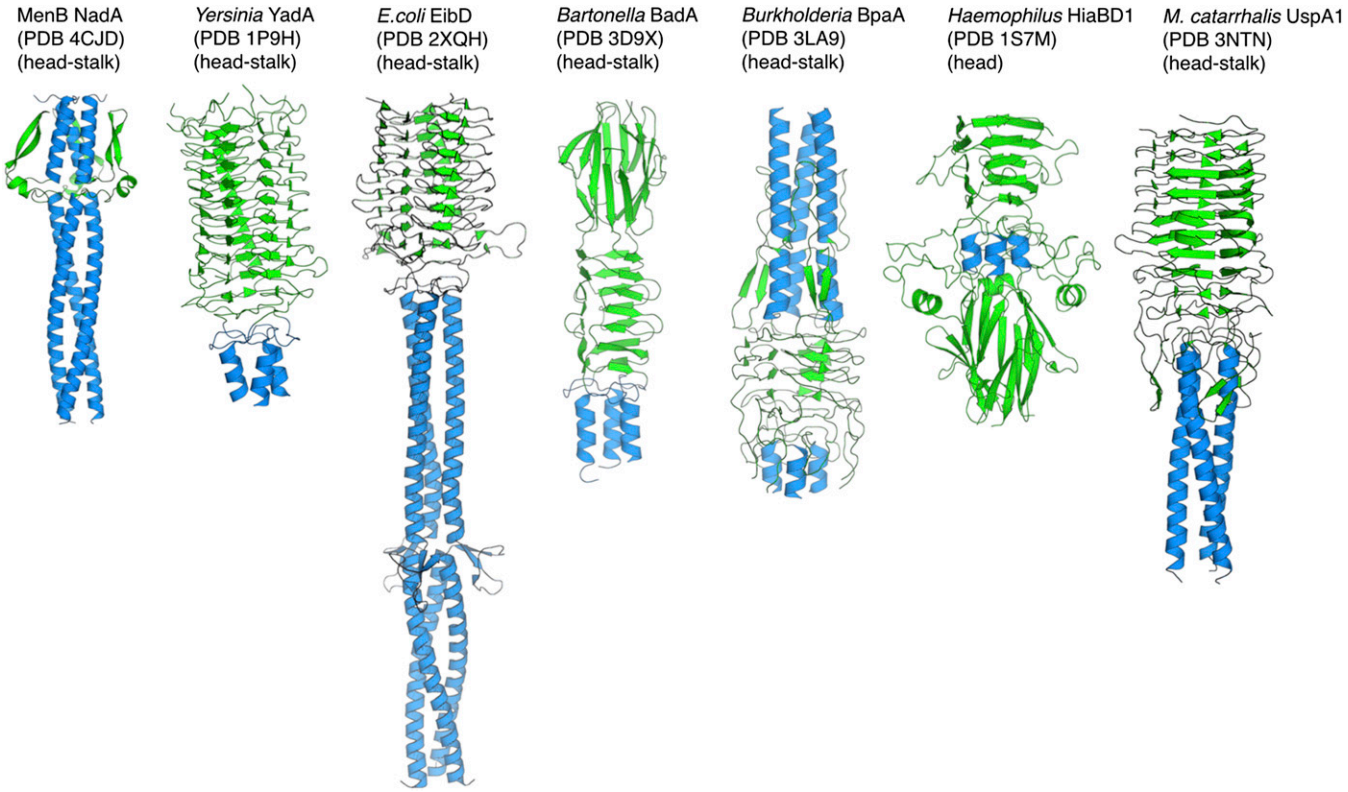

Fig. S7. Comparison of NadA with other known structures of trimeric autotransporter adhesins. β-Sheet and α-helical structures are shown as green and blue cartoons, respectively.

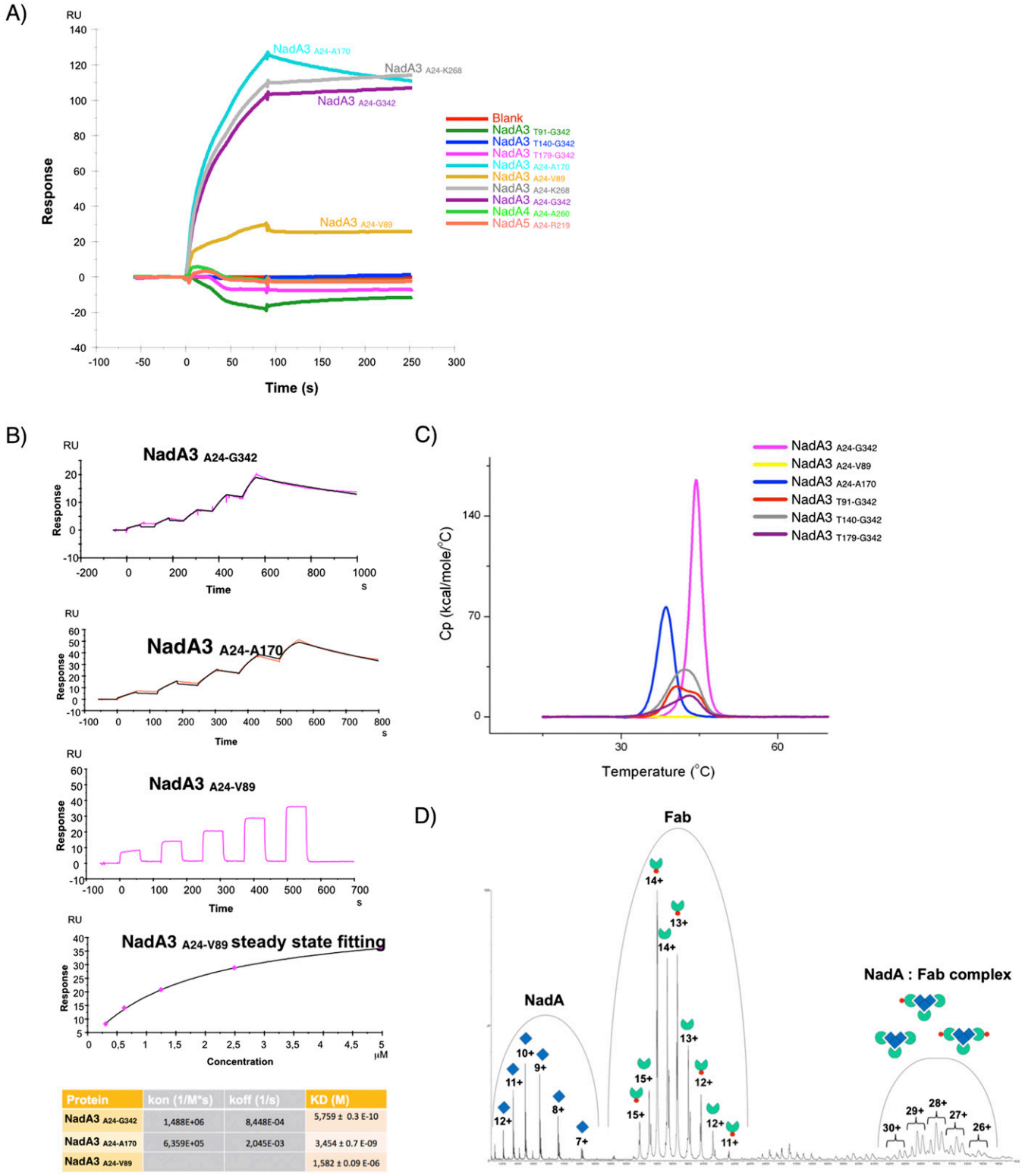

Protein	kon (1/M*s)	koff (1/s)	KD (M)
NadA3 A24-G342	1,488E+06	8,448E-04	5,759 ± 0.3 E-10
NadA3 A24-A170	6,359E+05	2,045E-03	3,454 ± 0.7 E-09
NadA3 A24-V89			1,582 ± 0.09 E-06

Fig. S8. Binding of mAb 33E8 to NadA3. (*A*) The affinity of NadA fragments for immobilized mAb 33E8 was assessed by single injections at 100-nM concentration. High binding responses (RU >100) were observed for NadA3 clones A24–G342, A24–K268, and A24–A170. Some residual binding to $NadA3_{A24–V89}$ was observed also (30 RU). Essentially no binding was observed to NadA3 clones T91–G342, T140–G342, T179–G342, to NadA4 clone A24–A260, or to NadA5 A24–R220. (*B*) SPR sensorgrams for SCK experiments showing that full-length $NadA3_{A24–G342}$ and $NadA3_{A24–A170}$ bind to mAb 33E8 with low-nanomolar affinity, whereas $NadA3_{A24–V89}$ shows an ∼1,000-fold weaker binding which required a steady-state fitting analysis. Experimental data (colored lines) and the calculated curves (black lines) were fitted to a 1:1 binding model. A table summarizing the kinetic binding parameters determined above is shown also. (*C*) DSC profiles of NadA clones used for studying the binding of mAb 33E8. A large peak with T_m = 44 °C (magenta) shows that the $NadA3_{A24–G342}$ is stably folded. Smaller peaks were observed with T_m = 38 °C for clone $NadA3_{A24–T170}$ (blue) and T_m 40–43 °C for the NadA3 clones T91–G342, T140–G342, and T179–G342

Legend continued on following page

(red, gray, and purple), indicating that these clones retain tertiary structure but are slightly less stable than the full-length construct. The $NadA3_{A24–V89}$ protein displayed a completely flat DSC profile (yellow) with no melting transition, indicating that it does not have a stable tertiary structure, i.e., is likely to be unfolded. (*D*) Stoichiometry of the binding of NadA to Fab 33E8 by nondenaturing nanoelectrospray MS. The nano-ESI mass spectrum of the complex $NadA3_{A24–A170}$:Fab 33E8 under native conditions is shown. The protein and the Fab also are present alone as dissociated species because of the ionization conditions in nondenaturing MS. The NadA monomer is represented by the charged state series from +7 to +11 in the 1,250–2,600 *m/z* range with a corresponding molecular mass of 16.9 kDa. The Fab, which exists in different species, probably because of unspecific cleavage of the relative mAb 33E8, corresponds to the charged state series from +11 to +15 in the 2,800–4,400 *m/z* range with a molecular mass ranging from 47.4–49.7 kDa. The measured molecular mass of the NadA trimer bound to three Fabs, ranging from 193.5–197.2 kDa, correlates with the expected mass of the different complex combinations and is reported by the charged state series from +26 to +30 in the 6,300–7,750 *m/z* range. All the NadA trimer apparently is bound to the Fabs and is not present in the spectrum.

Table S1. Data collection, phasing, and refinement statistics for the $NadA5_{A24-R220}$ iodide dataset

Crystal	
Space group	*R* 32 (155)
Cell dimensions	
a, b, c, Å	51.2, 51.2, 577.9
α, β, γ, °	90, 90, 120
Data collection	
Wavelength, Å	1.53998
Resolution limits, Å*	48.1–2.06 (2.18–2.06)
Total reflections*	330,567 (34,068)
Unique reflections*	34,971 (5,387)
R_{sym}, %*,†	6.2 (82.6)
I/σ, I*	22.75 (2.18)
Completeness, %*	99.2 (95.4)
Redundancy*	9.4 (6.3)
Wilson B-factor, $Å^2$	34.8
Phasing and density modification‡	
Figure of merit	0.352
Overall score	59.04 ± 6.96
R-factor, %	27.38
Map skew	0.23
Refinement	
Resolution, Å	48.1–2.06
No. reflections	34,948
R_{work}/R_{free}§	18.2/20.7
No. atoms	
Protein	905
Ligands/ions	4
Water	100
B-factors	
Protein	42.3
Ligands/ions	50.1
Water	38.2
rmsd	
Bond lengths, Å	0.014
Bond angles, °	1.207
Clash score	1.68

*The highest-resolution shell is shown in parenthesis.
†$R_{sym} = \Sigma_{hkl} \Sigma_i |I_i(hkl) - <I(hkl)>| / \Sigma_{hkl} \Sigma_i I_i(hkl)$.
‡Data from *autosol* (3).
§$R_{work} = \Sigma||F(obs)| - |F(calc)|| / \Sigma|F(obs)|$; R_{free} = as for R_{work} but calculated for 5.0% of the total reflections that were chosen at random and omitted from refinement.